

## HOURGLASS STABILIZATION OF THE PENTAHEDRAL SOLID ELEMENT\*

S. MOHAMMADI<sup>1\*\*</sup> D. R. J. OWEN AND D. PERIC<sup>2</sup>

<sup>1</sup>Dept. of Civil Engineering, University of Tehran, I. R. of Iran  
Email: smoham@ut.ac.ir

<sup>2</sup>Dept. of Civil Engineering, University of Wales Swansea, UK

**Abstract** – A one point quadrature pentahedral solid element with hourglass stabilization is developed for large deformation analysis of elastoplastic solids. This type of element is particularly suited for analysis of shell-like structures where multiple fracturing without any predefined direction takes place in the shell surface. Thus, the element design is motivated by requirements of the analysis of delamination and fracture in multilayered composite shells. The element formulation and the hourglass control procedure are based on the standard assumed strain method for stabilization of solid elements previously developed by other researchers. Several numerical tests, from simple beam bending to fracture analysis of laminated plates have been carried out to assess the performance of the element.

**Keywords** – Pentahedral element, Hourglass stabilization

### 1. INTRODUCTION

It is well known that a full integration of the internal forces and stiffness matrix arising in finite element analysis leads to difficulties in certain classes of problems. For instance, so-called volumetric locking is observed when the material is nearly incompressible. In addition, this scheme requires many computational operations to construct an element stiffness matrix and to obtain its internal forces. To remedy this situation, reduced integration schemes (RI) were introduced. However, a major drawback of the RI schemes is a mesh instability often known as *hourglassing*. They constitute a special case of the phenomenon known as kinematic or spurious zero-energy modes, and once activated they very quickly destroy the solutions. The selective reduced integration method (SRI), which was subsequently introduced, improved the drawbacks of the RI method, but it did not improve the computational efficiency.

Recently, Belytschko and his co-workers [1, 2] have developed a reduced integration method with hourglass control. This method maintains the computational efficiency of RI, avoiding its instability, and can be readily implemented. This method has been widely used for hourglass stabilization of 2D quadrilateral, plate, shell and solid elements.

The first attempts of this kind can be traced to Doherty *et al.* [3] who under-integrated the shear terms, suppressing the parasitic shear which causes the stiff behaviour of fully integrated quadrilaterals. However, these elements did not perform well for incompressible problems. Subsequently, Wilson *et al.* [4] constructed an element for both compressible and incompressible materials by adding incompatible bubble modes. The failure of the element to pass the patch test was remedied by Taylor *et al.* [5]. These elements comprise the underlying ideas for the later developed elements with hourglass control.

In earlier papers, Belytschko and his colleagues [2, 6, 7, 8] developed reduced integration elements by employing hourglass control methods. The main process of hourglass control has been constructed by introducing parameters for *artificial damping* and *artificial stiffness*; the latter being preferred [9]. In these works, the anti-hourglass mode vectors  $\gamma$ , which are derived by orthogonal conditions to preserve consistency, play an important part in the construction of a stabilization stiffness matrix and an additional correction force vector to avoid hourglass phenomena.

---

\*Received by the editors November 31, 2001 and in final revised form December 7, 2003

\*\*Corresponding author

Unfortunately, the magnitudes of the associated generalized stresses are governed by user-input hourglass control parameters. These parameters are usually chosen to be just large enough to prevent hourglassing, so this approach to stabilization is often called *perturbation hourglass control* [10]. However, coarse mesh solutions of bending dominated problems can be quite sensitive to the magnitude of the stabilization parameter. More importantly, the stabilization does not project out volumetric strains, so for incompressible materials it is possible for the element to become quite stiff or even lock as the stabilization parameter is increased. This is particularly important in the nonlinear range where many materials are almost incompressible [11].

In the following years, efforts focused on determining the control value of the hourglass control parameters (Stainier & Ponthot, [9]). Belytschko *et al.* [2, 8] introduced the idea of using a variational form of the three field Hu-Washizu principle, while Liu *et al.* [12, 13] proposed using a Taylor development of the strain rate. In this alternative approach the strain field is projected to eliminate the volumetric locking. This methodology can be considered as a special case of the  $\mathbf{B}$ -bar ( $\bar{\mathbf{B}}$ ) method, in which the gradient matrix  $\mathbf{B}$  of the standard displacement element is replaced by an assumed gradient matrix  $\bar{\mathbf{B}}$ . In other words, the standard  $\mathbf{B}$  matrix is projected onto a smaller space to eliminate the hourglass and locking phenomena both in a mathematical and physical sense [14].

Further contributions to the field were made by Koh and Kikuchi [15], Jetteur and Cescotto [16] among others. Koh and Kikuchi [15] developed 8-node bricks with directional reduced integration, which are effective for certain types of shells and beams. However, it can be shown that these elements are very sensitive to mesh distortion in the thin plate limit, so the elements can not be used as general purpose shell or plate elements. It appears from these studies that general three-dimensional elements, when distorted, will not perform well for plates and shells. Therefore, the enforcement of a structural hypothesis, such as the Kirchhoff or Mindlin-Reissner hypothesis, is crucial for good performance in thin plates and shells [11]. Liu *et al.* [17] proposed a new simple approach which is called the “multi-point quadrature scheme”, in which two quadrature points were used for a 4-node quadrilateral element in elastoplastic dynamic analysis by an explicit time integration scheme. However, the selection of the proper integration points for other elements in 3D has remained unresolved.

Belytschko and Bindeman [11] developed uniform reduced integration elements by the assumed strain method introduced by Simo and Hughes [18] to build a strain field avoiding the locking phenomenon by including shear locking. They extended their element to nonlinear problems in which an additional correction nodal force vector is required, and is then carried out in a corotational system. However, the choice of a corotational formulation for general 3D problems is not straightforward [11]. They have shown that the Simo-Hughes form of the Hu-Washizu variational principle is far more concise and the results differ little from the more complicated forms which ensue from the complete application of the Hu-Washizu variational principle [1].

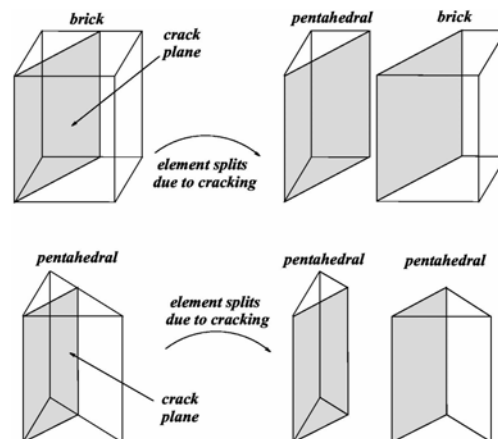


Fig. 1. Geometric crack modelling for 8-node brick and 6-node pentahedral elements

An 8-node brick element with mixed formulation for large deformation analysis has recently been developed by Li and Cescotto [19] which uses the same approach as Belytschko and Bindeman [11] and reportedly passes the large strain patch tests and guarantees stability and convergence. It has the correct rank of the stiffness matrix so that the hourglass modes can be avoided completely.

For a general 3D analysis of structures, 8-node solid elements are frequently used and preferred to other simple solid elements. However, in special circumstances, other solid elements may effectively be used. For example, pentahedral elements sometimes appear in relatively thick shell analysis as a substitute for triangular shell elements [20]. Here, the pentahedral element has been developed as an essential part of an element-split fracturing algorithm to be used in an advanced combined finite/discrete element analysis to investigate the formation, propagation and interaction of cracks and interlaminar delaminations in composites due to impact loadings [21, 22]. The impact analysis is performed using an explicit time integration scheme neglecting any wave propagation effects.

The 8-node brick solid element could not be used in such an approach due to the creation of various types of elements (brick and pentahedral elements) from geometric modelling of a crack inside a damaged element (see Fig. 1). In contrast, splitting a pentahedral element creates only similar types of elements. In the following, a one point quadrature formulation for the 6-node pentahedral element is described which is mainly based on the work by Belytschko and Bindeman [11] and Li and Cescotto [19] for an 8-node brick element. Several numerical tests from simple beam bending to fracture analysis of laminated plates have been carried out to assess the performance of the element.

## 2. FINITE ELEMENT INTERPOLATION AND DEFORMATION MODES

### a) Shape functions

Figure 2 defines three coordinate systems, global XYZ, local xyz and curvilinear  $\xi\eta\zeta$ , required in the formulation of the pentahedral element. All calculations are carried out on the local corotational system and then transformed to global vectors for updating the global quantities according to the explicit time integration scheme.

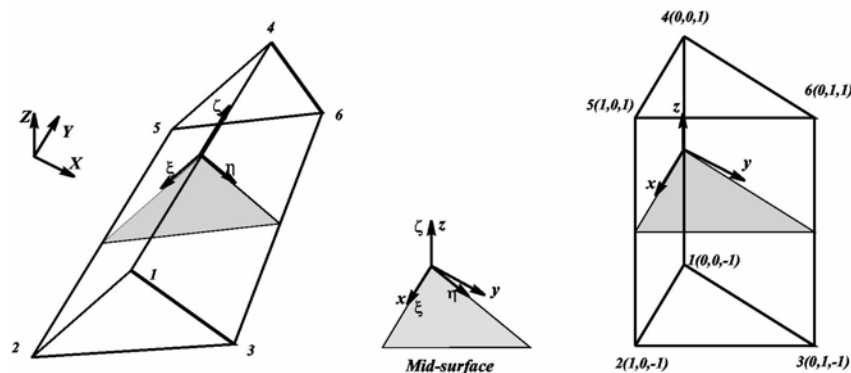


Fig. 2. Pentahedral element. Global XYZ, local xyz and curvilinear  $\xi\eta\zeta$  coordinate systems

The basic shape functions are obtained by multiplying the basis functions of a three node element by an appropriate function along the  $\zeta$  direction, i.e.

$$\begin{aligned}
 N_i &= \frac{1}{2}(1-\xi)(1-\eta)(1+\zeta\zeta_i) & i = 1,4 \\
 N_i &= \frac{1}{2}\xi(1+\zeta\zeta_i) & i = 2,5 \\
 N_i &= \frac{1}{2}\eta(1+\zeta\zeta_i) & i = 3,6
 \end{aligned} \tag{1}$$

For general pentahedral elements, the most obvious integration pattern is a combination of an appropriate triangular array in two dimensions and a Gauss distribution in the third direction. For the present case of the 6-node element, each triangular face requires only a single integration point to evaluate its constant strain states. However, even by ignoring the spurious modes along the thickness, a spurious mode corresponding to in-plane rotation of one triangular face relative to the other exists. So the minimum practical pattern of integration points for this element which avoids spurious modes is a  $3 \times 2$  pattern [20]. Obviously, this pattern is not economically acceptable in the context of an explicit approach, therefore a one point quadrature with hourglass stabilization is adopted.

### b) Geometry Description

Adopting the isoparametric interpolation, the spatial coordinates of a given point  $(\xi, \eta, \zeta)$  within the element may be expressed as

$$x_i = \sum_{A=1}^6 N_A X_{iA}, \quad i=1,2,3 \quad (2)$$

where  $\mathbf{X}_i = (X_{iA})^T = (X_{i1}, X_{i2}, X_{i3}, X_{i4}, X_{i5}, X_{i6})^T$  is a vector of nodal coordinates. After some manipulations the above expression may be written as

$$x_i = (\mathbf{t}^T + \mathbf{I}_1^T \xi + \mathbf{I}_2^T \eta + \mathbf{I}_3^T \zeta + \mathbf{m}_1^T \xi \zeta + \mathbf{m}_2^T \eta \zeta) \mathbf{X}_i \quad (3)$$

where

$$\mathbf{t}^T = \frac{1}{2}[1,0,0,1,0,0], \quad \mathbf{I}_1^T = \frac{1}{2}[-1,1,0,-1,1,0], \quad \mathbf{I}_2^T = \frac{1}{2}[-1,0,1,1,0,1], \quad \mathbf{I}_3^T = \frac{1}{2}[-1,0,0,1,0,0],$$

$$\mathbf{m}_1^T = \frac{1}{2}[1,-1,0,-1,1,0], \quad \mathbf{m}_2^T = \frac{1}{2}[1,0,-1,-1,0,1]$$

### c) Kinematic description

**1. Displacements:** A similar approach for the displacement vector  $u$  leads to

$$u_i = (\mathbf{t}^T + \mathbf{I}_1^T \xi + \mathbf{I}_2^T \eta + \mathbf{I}_3^T \zeta + \mathbf{m}_1^T \xi \zeta + \mathbf{m}_2^T \eta \zeta) \mathbf{d}_i \quad (4)$$

where  $\mathbf{d}_i$  represents the nodal displacement vector. The physical meaning of these deformation modes may be better understood from Figs. 3 and 4 in which deformation modes along the  $x_1$  and  $x_3$  axes have been considered, respectively.

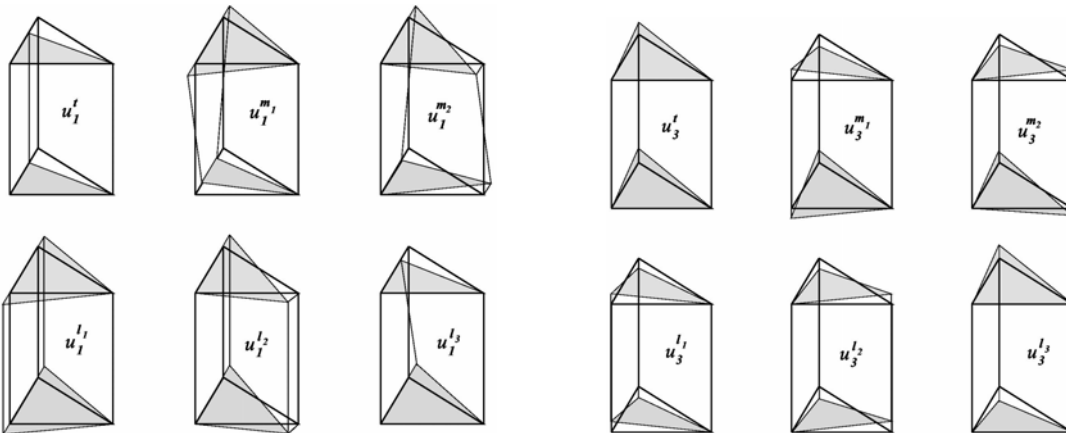


Fig. 3. Modes of deformation along the  $x_1$  axis

Fig. 4. Modes of deformation along the  $x_3$  axis

By substituting the physical coordinates instead of the curvilinear coordinates in Eq. (3), a more appropriate format is achieved

$$u_i = (\mathbf{g}_0^T + x_j \mathbf{b}_j^T + h_\alpha \boldsymbol{\gamma}_\alpha^T) \mathbf{d}_i \quad (5)$$

where

$$\mathbf{b}_j = N_{,j}(\mathbf{0}) = \frac{\partial N}{\partial x_j}(\mathbf{0}), \quad \mathbf{g}_0 = \mathbf{t} - (\mathbf{t}^T \mathbf{X}_j) \mathbf{b}_j, \quad \boldsymbol{\gamma}_\alpha = \mathbf{m}_\alpha - (\mathbf{m}_\alpha^T \mathbf{X}_j) \mathbf{b}_j, \quad h_1 = \xi \zeta, \quad h_2 = \eta \zeta$$

where  $i, j = 1, 2, 3$  and  $\alpha = 1, 2$  and the summation rule over the repeated indices is implied throughout the paper, unless otherwise stated. The following orthogonality conditions are readily verified;

$$\mathbf{b}_i^T \mathbf{t} = \mathbf{b}_i^T \mathbf{m}_\alpha = 0, \quad \mathbf{t}^T \mathbf{m}_\alpha = \mathbf{m}_\alpha^T \mathbf{t} = 0, \quad \mathbf{b}_i^T \mathbf{X}_j = \delta_{ij}, \quad \bar{\mathbf{h}}_\alpha^T \bar{\mathbf{h}}_\beta = 2\delta_{\alpha\beta} \quad (6)$$

where  $\bar{\mathbf{h}}_\alpha$  is a vector of the nodal values of  $h_\alpha$

$$\bar{\mathbf{h}}_\alpha^T = (h_{\alpha 1}, h_{\alpha 2}, h_{\alpha 3}, h_{\alpha 4}, h_{\alpha 5}, h_{\alpha 6}) \quad (7)$$

**2. Strain Tensor:** Assuming that small strain approximations are applicable, the strain-displacement relations are expressed as

$$u_{i,j} = \frac{\partial u_i}{\partial x_j} \quad (8)$$

$$u_{i,j} = (\mathbf{b}_j^T + h_{\alpha,j} \boldsymbol{\gamma}_\alpha^T) \mathbf{d}_i \quad (9)$$

So the strain-displacement matrix  $\mathbf{B}$  is defined

$$\begin{bmatrix} u_{1,1} \\ u_{2,2} \\ u_{3,3} \\ u_{1,2} + u_{2,1} \\ u_{2,3} + u_{3,2} \\ u_{3,1} + u_{1,3} \end{bmatrix} = \mathbf{B} \mathbf{d} = \begin{bmatrix} \mathbf{b}_1^T + h_{\alpha,1} \boldsymbol{\gamma}_\alpha^T & \mathbf{0} & \mathbf{0} \\ \mathbf{0} & \mathbf{b}_2^T + h_{\alpha,2} \boldsymbol{\gamma}_\alpha^T & \mathbf{0} \\ \mathbf{0} & \mathbf{0} & \mathbf{b}_3^T + h_{\alpha,3} \boldsymbol{\gamma}_\alpha^T \\ \mathbf{b}_2^T + h_{\alpha,2} \boldsymbol{\gamma}_\alpha^T & \mathbf{b}_1^T + h_{\alpha,1} \boldsymbol{\gamma}_\alpha^T & \mathbf{0} \\ \mathbf{0} & \mathbf{b}_3^T + h_{\alpha,3} \boldsymbol{\gamma}_\alpha^T & \mathbf{b}_2^T + h_{\alpha,2} \boldsymbol{\gamma}_\alpha^T \\ \mathbf{b}_3^T + h_{\alpha,3} \boldsymbol{\gamma}_\alpha^T & \mathbf{0} & \mathbf{b}_1^T + h_{\alpha,1} \boldsymbol{\gamma}_\alpha^T \end{bmatrix} \begin{bmatrix} \mathbf{d}_1 \\ \mathbf{d}_2 \\ \mathbf{d}_3 \end{bmatrix} \quad (10)$$

or in compact form

$$\boldsymbol{\varepsilon} = \bar{\boldsymbol{\varepsilon}} + \boldsymbol{\varepsilon}_h = (\bar{\mathbf{B}} + \mathbf{B}_h) \mathbf{d} \quad (11)$$

with

$$\boldsymbol{\varepsilon}_h = \mathbf{B}_h \mathbf{d} = \mathbf{h} \boldsymbol{\Gamma} \mathbf{d} \quad (12)$$

where  $\bar{\mathbf{B}}$  is the constant part and  $\mathbf{B}_h$  is the hourglass stabilization part of the  $\mathbf{B}$  matrix

$$\mathbf{B}_h = \begin{bmatrix} h_{\alpha,1} \boldsymbol{\gamma}_\alpha^T & \mathbf{0} & \mathbf{0} \\ \mathbf{0} & h_{\alpha,2} \boldsymbol{\gamma}_\alpha^T & \mathbf{0} \\ \mathbf{0} & \mathbf{0} & h_{\alpha,3} \boldsymbol{\gamma}_\alpha^T \\ h_{\alpha,2} \boldsymbol{\gamma}_\alpha^T & h_{\alpha,1} \boldsymbol{\gamma}_\alpha^T & \mathbf{0} \\ \mathbf{0} & h_{\alpha,3} \boldsymbol{\gamma}_\alpha^T & h_{\alpha,2} \boldsymbol{\gamma}_\alpha^T \\ h_{\alpha,3} \boldsymbol{\gamma}_\alpha^T & \mathbf{0} & h_{\alpha,1} \boldsymbol{\gamma}_\alpha^T \end{bmatrix} \quad (13)$$

and

$$\mathbf{h} = \begin{bmatrix} h_{1,1} & 0 & 0 & h_{2,1} & 0 & 0 \\ 0 & h_{1,2} & 0 & h_{2,2} & 0 & 0 \\ 0 & 0 & h_{1,3} & 0 & 0 & h_{2,3} \\ h_{1,2} & h_{1,1} & 0 & h_{2,2} & h_{2,1} & 0 \\ 0 & h_{1,3} & h_{1,2} & 0 & h_{3,1} & h_{2,2} \\ h_{1,3} & 0 & h_{1,1} & h_{2,3} & 0 & h_{2,1} \end{bmatrix}, \quad \boldsymbol{\Gamma} = \begin{bmatrix} \boldsymbol{\gamma}_1 & \mathbf{0} & \mathbf{0} \\ \mathbf{0} & \boldsymbol{\gamma}_1 & \mathbf{0} \\ \mathbf{0} & \mathbf{0} & \boldsymbol{\gamma}_1 \\ \boldsymbol{\gamma}_2 & \mathbf{0} & \mathbf{0} \\ \mathbf{0} & \boldsymbol{\gamma}_2 & \mathbf{0} \\ \mathbf{0} & \mathbf{0} & \boldsymbol{\gamma}_2 \end{bmatrix} \quad (14)$$

To evaluate the  $h_{\alpha,j}$  terms, the chain rule may effectively be used

$$\frac{\partial(\bullet)}{\partial x_j} = \frac{\partial(\bullet)}{\partial \xi} \frac{\partial \xi}{\partial x_j} + \frac{\partial(\bullet)}{\partial \eta} \frac{\partial \eta}{\partial x_j} + \frac{\partial(\bullet)}{\partial \zeta} \frac{\partial \zeta}{\partial x_j} \quad (15)$$

which requires the evaluation of the Jacobian matrix

$$\mathbf{J} = \begin{bmatrix} \frac{\partial \xi}{\partial x_1} & \frac{\partial \eta}{\partial x_1} & \frac{\partial \zeta}{\partial x_1} \\ \frac{\partial \xi}{\partial x_2} & \frac{\partial \eta}{\partial x_2} & \frac{\partial \zeta}{\partial x_2} \\ \frac{\partial \xi}{\partial x_3} & \frac{\partial \eta}{\partial x_3} & \frac{\partial \zeta}{\partial x_3} \end{bmatrix} \quad (16)$$

which eventually results in evaluation of the derivatives of the hourglass modes

$$h_{1,i} = \zeta J_{i2}^{-1} + \eta J_{i3}^{-1}, \quad h_{2,i} = \zeta J_{i1}^{-1} + \xi J_{i3}^{-1} \quad (17)$$

where  $J_{ij}^{-1}$  is the  $ij$  component of the  $\mathbf{J}^{-1}$  matrix.

### 3. ASSUMED STRAIN FIELD AND STABILIZATION PROCEDURE

As emphasized by Belytschko and Bindeman [11] and later by Li and Cescotto [19], if Eq. (11) is used as the discretized strain field, the element can lock for incompressible materials and exhibit excessive energy in shear mode for bending dominated problems. To remedy this situation, an *assumed strain* field is employed for the non-constant part of the strain field.

#### a) Assumed strain field

First, the hourglass strain field is decomposed into normal and shear components

$$\boldsymbol{\varepsilon}_h = \boldsymbol{\varepsilon}_h^n + \boldsymbol{\varepsilon}_h^s \quad (18)$$

in which the normal term is decomposed into deviatoric and volumetric parts

$$\boldsymbol{\varepsilon}_h^n = \boldsymbol{\varepsilon}_h^d + \boldsymbol{\varepsilon}_h^v \quad (19)$$

To eliminate volumetric locking, the strain field must be designed (projected) so that in the hourglass mode the dilatation of the projected strain field vanishes throughout the element. Hence, the volumetric part  $\boldsymbol{\varepsilon}_h^v$  of the normal component of the hourglass strain field  $\boldsymbol{\varepsilon}_h^n$  is neglected [11, 19]. The strain-displacement matrix  $\mathbf{B}_h^d$  then takes the form

$$\mathbf{B}_h^d = \frac{1}{3} \begin{bmatrix} 2h_{\alpha,1}\boldsymbol{\gamma}_\alpha^T & -h_{\alpha,2}\boldsymbol{\gamma}_\alpha^T & -h_{\alpha,3}\boldsymbol{\gamma}_\alpha^T \\ -h_{\alpha,1}\boldsymbol{\gamma}_\alpha^T & 2h_{\alpha,2}\boldsymbol{\gamma}_\alpha^T & -h_{\alpha,3}\boldsymbol{\gamma}_\alpha^T \\ -h_{\alpha,1}\boldsymbol{\gamma}_\alpha^T & -h_{\alpha,2}\boldsymbol{\gamma}_\alpha^T & 2h_{\alpha,3}\boldsymbol{\gamma}_\alpha^T \\ \mathbf{0} & \mathbf{0} & \mathbf{0} \\ \mathbf{0} & \mathbf{0} & \mathbf{0} \\ \mathbf{0} & \mathbf{0} & \mathbf{0} \end{bmatrix} \quad (20)$$

For the shear part, the shear parameters are introduced to avoid shear locking problems

$$\mathbf{B}_h^s = \begin{bmatrix} \mathbf{0} & \mathbf{0} & \mathbf{0} \\ \mathbf{0} & \mathbf{0} & \mathbf{0} \\ \mathbf{0} & \mathbf{0} & \mathbf{0} \\ \beta_{12}h_{\alpha,2}\boldsymbol{\gamma}_\alpha^T & \beta_{12}h_{\alpha,1}\boldsymbol{\gamma}_\alpha^T & \mathbf{0} \\ \mathbf{0} & \beta_{23}h_{\alpha,3}\boldsymbol{\gamma}_\alpha^T & \beta_{23}h_{\alpha,2}\boldsymbol{\gamma}_\alpha^T \\ \beta_{13}h_{\alpha,3}\boldsymbol{\gamma}_\alpha^T & \mathbf{0} & \beta_{13}h_{\alpha,1}\boldsymbol{\gamma}_\alpha^T \end{bmatrix} \quad (21)$$

The  $\beta_{ij}$  parameters may be determined from the element geometry according to the following rules:

$$\beta_{12} = \frac{\min(x_{mean}, y_{mean})}{\max(x_{mean}, y_{mean})}, \quad \beta_{23} = \frac{\min(y_{mean}, z_{mean})}{\max(y_{mean}, z_{mean})}, \quad \beta_{13} = \frac{\min(x_{mean}, z_{mean})}{\max(x_{mean}, z_{mean})} \quad (22)$$

where

$$Y_{mean} = \frac{1}{6} (|Y_{15}| + |Y_{24}| + |Y_{26}| + |Y_{35}| + |Y_{16}| + |Y_{34}|) \quad (23)$$

with  $Y = x, y, z$  and  $Y_{ij} = Y_i - Y_j$ .

For bending dominated problems shear locking is possible when  $\beta_{ij} = 1$ , whereas  $\beta_{ij} = 0$  is associated with torsion dominated problems in which only shear energy exists. Therefore, Eqs. (18) and (19) describe a strain field that may behave well for both thin and thick structures thus avoiding hourglass locking for bending and torsional deformations. The hourglass strain field may be expressed as

$$\boldsymbol{\varepsilon}_h = \boldsymbol{\varepsilon}_h^d + \boldsymbol{\varepsilon}_h^s \quad (24)$$

with a similar expression for the corresponding hourglass mode derivatives, ( $\boldsymbol{\varepsilon}_h = \mathbf{h}\boldsymbol{\Gamma} \mathbf{d}$ )

$$\mathbf{h} = \mathbf{h}_d + \mathbf{h}_s \quad (25)$$

where  $\mathbf{h}$  and  $\boldsymbol{\Gamma}$  are defined in Eqs. (14), and the normal, deviatoric and shear parts of  $\mathbf{h}$  may be defined as

$$\mathbf{h}_n = \begin{bmatrix} h_{1,1} & 0 & 0 & h_{2,1} & 0 & 0 \\ 0 & h_{1,2} & 0 & 0 & h_{2,2} & 0 \\ 0 & 0 & h_{1,3} & 0 & 0 & h_{2,3} \\ 0 & 0 & 0 & 0 & 0 & 0 \\ 0 & 0 & 0 & 0 & 0 & 0 \\ 0 & 0 & 0 & 0 & 0 & 0 \end{bmatrix}, \quad \mathbf{h}_d = \frac{1}{3} \begin{bmatrix} 2h_{1,1} & -h_{1,2} & -h_{1,3} & 2h_{2,1} & -h_{2,2} & -h_{2,3} \\ -h_{1,1} & 2h_{1,2} & -h_{1,3} & -h_{2,1} & 2h_{2,2} & -h_{2,3} \\ -h_{1,1} & -h_{1,2} & 2h_{1,3} & -h_{2,1} & -h_{2,2} & 2h_{2,3} \\ 0 & 0 & 0 & 0 & 0 & 0 \\ 0 & 0 & 0 & 0 & 0 & 0 \\ 0 & 0 & 0 & 0 & 0 & 0 \end{bmatrix}$$

$$\mathbf{h}_s = \begin{bmatrix} 0 & 0 & 0 & 0 & 0 & 0 \\ 0 & 0 & 0 & 0 & 0 & 0 \\ 0 & 0 & 0 & 0 & 0 & 0 \\ \beta_{12}h_{1,2} & \beta_{12}h_{1,1} & 0 & \beta_{12}h_{2,2} & \beta_{12}h_{2,1} & 0 \\ 0 & \beta_{23}h_{1,3} & \beta_{23}h_{1,2} & 0 & \beta_{23}h_{3,1} & \beta_{23}h_{2,2} \\ \beta_{13}h_{1,3} & 0 & \beta_{13}h_{1,1} & \beta_{13}h_{2,3} & 0 & \beta_{13}h_{2,1} \end{bmatrix}$$

For later usage, it is convenient to define

$$\boldsymbol{\varepsilon}_{gh} = \boldsymbol{\Gamma} \mathbf{d} \quad (26)$$

as the *generalized hourglass strain*.

### b) Stabilization procedure for linear elastic problems

The stabilization force vector may be evaluated from the stabilization stiffness matrix

$$\mathbf{f}_{stab} = \mathbf{K}_{stab} \mathbf{d}, \quad \text{and} \quad \mathbf{K}_{stab} = \int_{\Omega} \mathbf{B}_h^T \mathbf{C} \mathbf{B}_h d\Omega \quad (27)$$

Here, the approach adopted by Li and Cescotto [19] is followed. For linear elastic materials, the stress field can be expressed as

$$\boldsymbol{\sigma} = \mathbf{C}^e \boldsymbol{\varepsilon} = \mathbf{C}^e (\boldsymbol{\varepsilon}_0 + \boldsymbol{\varepsilon}_h) \quad (28)$$

where

$$\mathbf{C}^e = \frac{2G}{(1-2\nu)} \begin{bmatrix} 1-\nu & \nu & \nu & 0 & 0 & 0 \\ \nu & 1-\nu & \nu & 0 & 0 & 0 \\ \nu & \nu & 1-\nu & 0 & 0 & 0 \\ 0 & 0 & 0 & \frac{(1-2\nu)}{2} & 0 & 0 \\ 0 & 0 & 0 & 0 & \frac{(1-2\nu)}{2} & 0 \\ 0 & 0 & 0 & 0 & 0 & \frac{(1-2\nu)}{2} \end{bmatrix}$$

The total stress is composed of two parts

$$\boldsymbol{\sigma} = \boldsymbol{\sigma}_0 + \boldsymbol{\sigma}_h \quad (29)$$

where

$$\boldsymbol{\sigma}_0 = \mathbf{C}^e \boldsymbol{\varepsilon}_0 \quad (30)$$

$$\boldsymbol{\sigma}_h = \mathbf{C}^e \mathbf{h} \boldsymbol{\varepsilon}_{gh} \quad (31)$$

Applying Eq. (25) and considering the following properties for linear elastic materials

$$\mathbf{C}^e \mathbf{h}_d = 2G \mathbf{h}_d, \quad \mathbf{C}^e \mathbf{h}_s = G \mathbf{h}_s \quad (32)$$

Equation (31) results in

$$\boldsymbol{\sigma}_h = \mathbf{h}_\sigma \boldsymbol{\sigma}_{gh} \quad (33)$$

where  $\boldsymbol{\sigma}_{gh}$  is the *generalized hourglass stress*

$$\boldsymbol{\sigma}_{gh} = 2G \boldsymbol{\varepsilon}_{gh} \quad (34)$$

and  $\mathbf{h}_\sigma = \mathbf{h}_d + \frac{1}{2} \mathbf{h}_s$

where  $\mathbf{h}_\sigma$  may be interpreted as the interpolation function of the generalized hourglass stress in the element.

### c) Stabilization procedure for nonlinear applications

To extend the formulation for nonlinear application, the variational form of the Hu-Washizu principle is used, where the displacements, strains and stresses are used as the independent test functions [18]

$$\int_{\Omega} \delta \boldsymbol{\varepsilon}^T (\boldsymbol{\Sigma} - \boldsymbol{\sigma}) d\Omega + \int_{\Omega} \delta \boldsymbol{\sigma}^T (\nabla^s \mathbf{u} - \boldsymbol{\varepsilon}) d\Omega + \int_{\Omega} \delta (\nabla^s \mathbf{u})^T \boldsymbol{\sigma} d\Omega - \delta \mathbf{d}^T \mathbf{f}^{ext} = 0 \quad (35)$$

where  $\Omega$  is the current domain,  $\nabla^s \mathbf{u}$  is the symmetric part of the displacement gradient field,  $\boldsymbol{\varepsilon}$  is the discretized strain field (assumed),  $\boldsymbol{\sigma}$  is the discretized stress field (assumed),  $\boldsymbol{\Sigma}$  is the Cauchy stress obtained from the strain field  $\boldsymbol{\varepsilon}$ ,  $\mathbf{f}^{ext}$  is the external load and  $\mathbf{d}$  is the nodal displacement.

Following standard argument, it may be shown that the first term results in expressions (30, 31, 34) for the total stress and generalized hourglass stress, while the second term results in expressions (11, 12, 26) for total strain and generalized hourglass strain (For a comprehensive discussion see [19]. Only the third term of Eq. (35) directly contributes to the internal force vector

$$\int_{\Omega} \delta (\nabla^s \mathbf{u})^T \boldsymbol{\sigma} d\Omega = \int_{\Omega} \delta \mathbf{d}^T (\overline{\mathbf{B}}^T + \Gamma^T \mathbf{h}_\Gamma^T) (\boldsymbol{\sigma}_0 + \mathbf{h}_\sigma \boldsymbol{\sigma}_{gh}) d\Omega \quad (36)$$

where  $\mathbf{h}_\Gamma = \mathbf{h}_n + \mathbf{h}_s$ . By defining

$$\mathbf{H} = \int_{\Omega} \mathbf{h}_\Gamma^T \mathbf{h}_\sigma d\Omega \quad (37)$$

Equation (36) becomes

$$\int_{\Omega} \delta (\nabla^s \mathbf{u})^T \boldsymbol{\sigma} d\Omega = \delta \mathbf{d}^T (\overline{\mathbf{B}}^T \boldsymbol{\sigma}_0 + \Gamma^T \mathbf{H} \boldsymbol{\sigma}_{gh}) \quad (38)$$

Thus, we have the equilibrium equation

$$\mathbf{f}^{\text{int}} - \mathbf{f}^{\text{ext}} = \mathbf{0} \quad (39)$$

where

$$\mathbf{f}^{\text{int}} = V \bar{\mathbf{B}}^T \boldsymbol{\sigma}_0 + \Gamma^T \mathbf{H} \boldsymbol{\sigma}_{gh}$$

The second part of the internal force vector is the hourglass contribution and is denoted

$$\mathbf{f}^h = \Gamma^T \mathbf{H} \boldsymbol{\sigma}_{gh} \quad (40)$$

For the purpose of implementation, Eqs. (37) and (40) have been expanded, resulting in the following explicit formulae ( $a, b = 1, 2$  and  $i, k, l = 1, 2, 3$  and  $j = 1, 2$  with no summation rule over repeated indices)

$$f_i^h = 2G\gamma_1 Q_{i1} + 2G\gamma_2 Q_{i2} \quad (41)$$

$$Q_{ij} = S_{i1}^{j1} \varepsilon_{11}^{gh} + S_{i2}^{j1} \varepsilon_{21}^{gh} + S_{i3}^{j1} \varepsilon_{31}^{gh} + S_{i1}^{j2} \varepsilon_{12}^{gh} + S_{i2}^{j2} \varepsilon_{22}^{gh} + S_{i3}^{j2} \varepsilon_{32}^{gh} \quad (42)$$

$$S_{ij}^{ab} = \left[ -\frac{1}{3} + \frac{1}{2} \beta_{ij}^2 \right] H_{ij}^{ab}, \quad S_{ii}^{ab} = \left( \frac{2}{3} \right) H_{ii}^{ab} + \left( \frac{1}{2} \beta_{il}^2 \right) H_{ll}^{ab} + \left( \frac{1}{2} \beta_{ik}^2 \right) H_{kk}^{ab}, \quad H_{ij}^{ab} = \int_{\Omega_e} h_{a,i} h_{b,j} d\Omega$$

The values of  $H_{ij}^{ab}$  are numerically evaluated at the gauss point.

As suggested by Belytschko *et al.* [1, 11], the value of the shear modulus  $G$  is updated for inelastic stress increments according to

$$2G = \sqrt{\frac{\Pi_{\Delta S}}{\Pi_{\Delta e}}} \quad (43)$$

where

$$\Pi_{\Delta S} = \frac{1}{2} \sum_{i=1}^3 \sum_{j=1}^3 \Delta S_{ij} \Delta S_{ij}, \quad \Pi_{\Delta e} = \frac{1}{2} \sum_{i=1}^3 \sum_{j=1}^3 \Delta e_{ij} \Delta e_{ij} \quad (44)$$

and  $\Delta S_{ij}$  and  $\Delta e_{ij}$  are components of the deviatoric part of the stress and strain increments, respectively, which are evaluated at the integration point.

#### 4. NUMERICAL VERIFICATION

In this section some of the test results are reviewed to assess the performance of this element within the context of an explicit dynamic analysis.

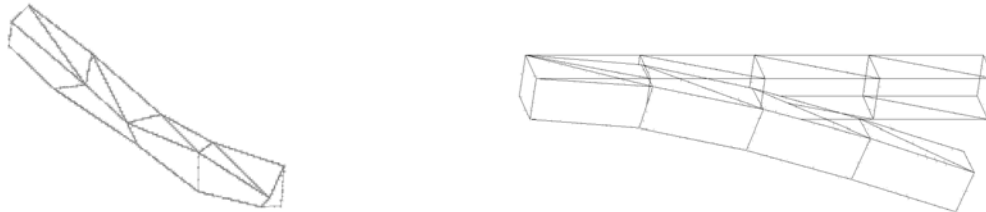


Fig. 5. Hourglass instability of the cantilever beam and its stabilized solution. ( $E = 210e9$ ,  $\nu = 0.1$ ,  $\rho = 7600$ ,  $length = 10$ ,  $width = 1$ ,  $height = 1$ ,  $load = 525e5$ )

##### a) Cantilever beam

A cantilever beam subjected to a constant edge loading is considered. This fundamental test is presented to demonstrate a simple view of how the stabilized element may prevent the hourglass instability of an elastically bending beam. The behavior of the element without any hourglass control is depicted in Fig. 5. The element fails at the very beginning of the analysis, however, with the hourglass control a very smooth deformed shape is achieved. Figure 6 compares the displacement history for the pentahedral and 8-node brick elements.

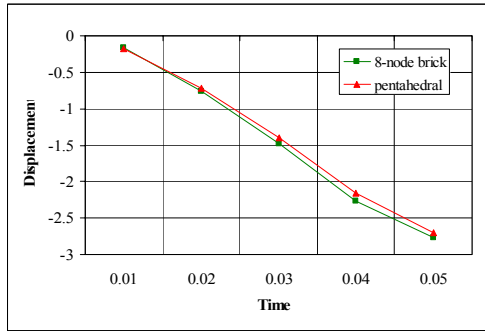


Fig. 6. Comparison of the free-end vertical displacement for 6-node and 8-node meshes

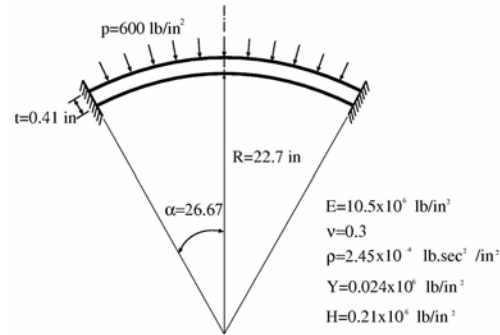


Fig. 7. Spherical shell

### b) Spherical shell

The geometric and material description of this standard test of shell elements [23] is depicted in Fig. 7. The pressure load is applied normally to the surface of the elements and its local direction and magnitude are kept constant during the analysis. Without any hourglass control, the analysis fails in the early timesteps, and the hourglass modes completely destroy the results of the analysis, as depicted in the figure. The results of deformation for a stabilized brick element and the present stabilized pentahedral element are compared in Fig. 9. The reference curve is taken from the analysis by quadrilateral shell elements based on Belytschko *et al.* [24].

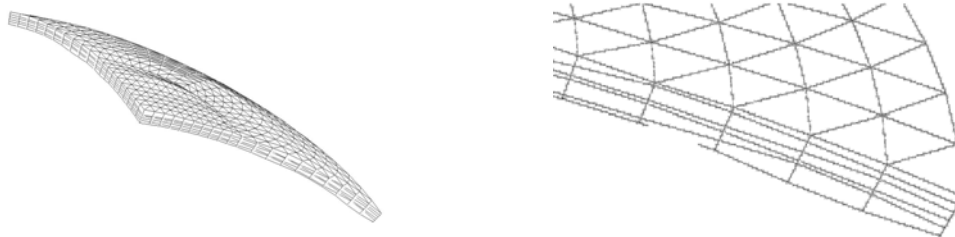


Fig. 8. Hourglass instability of the spherical shell

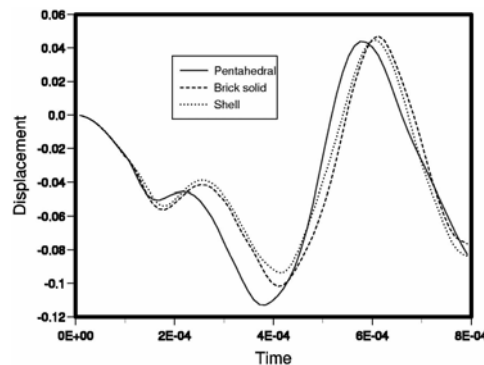


Fig. 9. Crown displacement history of the spherical shell for different finite element meshes

### c) Cylindrical panel loaded impulsively

A cylindrical panel was studied by Belytschko and Leviathan [10] to simulate the experimental results reported by Balmer and Witmer [25]. The geometry and mechanical properties of the structure are defined in Fig. 10. The impulsive loading with initial velocity  $v_0$  lasts 4 *m* sec. Due to symmetry, only one half of the structure is modelled and a 3D elastic perfectly plastic law based on the von Mises yield criterion and an associated flow rule is used. The permanent deformed shape of the cylinder is shown in Fig. 11. The displacement of the midpoint along the crown line of the cylinder is compared with the experimental results [25] and the numerical results obtained by Belytschko *et al.* [26, 10] (Fig. 12).

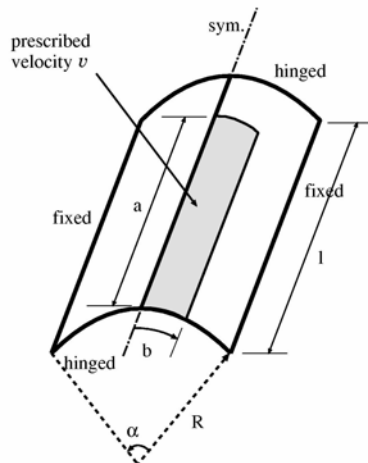


Fig. 10. Cylindrical panel. Geometry and mechanical properties

Cylindrical panel parameters	
$a = 10.205 \text{ in}$	$b = 1.54 \text{ in}$
$l = 12.56 \text{ in}$	$R = 2.9375 \text{ in}$
$t = 0.125 \text{ in}$	$\alpha = 120^\circ$
$E = 1.05e07$	$\nu = 0.33$
$\rho = 2.5e-04$	$v_0 = 5650 \text{ in/sec}$
$\sigma_y = 4.4e04 \text{ psi}$	$E_p = 0$

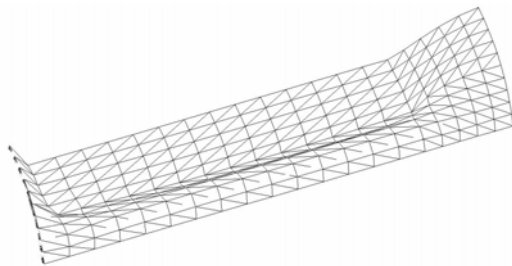


Fig. 11. Permanent deformation of the cylindrical panel

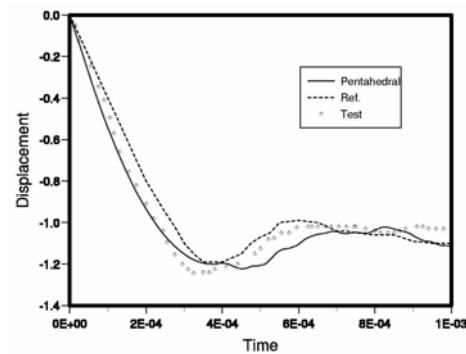


Fig. 12. Comparison of the displacement history of the crown of the cylinder at its midspan

#### d) Impact loading of a composite plate

A numerical simulation is undertaken to study the fracture and delamination behaviour of a laminated composite plate which is subjected to a high velocity impact at its centre. The impact loading is simulated by a triangular load applied from 0 to 5  $\mu\text{sec}$  with a peak force of 1kN. Figure 13 illustrates the geometry of the plate, and defines the material properties and other necessary information [27]. The composite ply pattern is assumed to be  $[+45_n, -45_n, +45_n, -45_n, +45_n]$ . Because of nonsymmetry, the whole plate has to be modelled.

An unstructured mesh of pentahedral elements is used for modelling the plate. A regular three-element mesh is used across the thickness of each layer. In this example, the possibility of fracture and delamination is not restricted to any particular region. At the starting point, over 30,000 elements and 25,000 points are used for the finite element modelling.

Figures 14-15 compare the fractured region (matrix cracking) of different layers at two different stages of the loading. Shaded regions in these figures represent the failed points of the mesh. Figure 16 illustrates the debonding patterns at different interfaces at the end of analysis. A special local remeshing technique is used for geometric modelling of a crack. Interactions between crack faces have been modelled using concepts of frictional contact mechanics [22].

## 5. CONCLUSIONS

A one point quadrature pentahedral solid element with hourglass stabilization has been developed as part of a combined finite/discrete element procedure to analyse the formation, propagation and interaction of cracks in solids due to impact loading. The element formulation and the hourglass control procedure are based on the assumed strain method. The element performs well in large deformation and nonlinear analysis. It is a

computationally inexpensive element and its main drawback is the fact that the number of elements are doubled in comparison to a brick element modelling of the same domain. Several numerical tests from simple beam bending to fracture analysis of laminated plates, have been carried out and confirmed as excellent performances of the element.

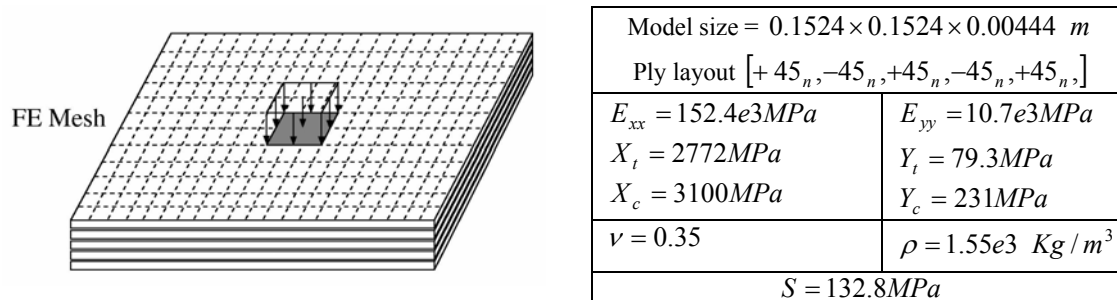


Fig. 13.  $[+45_n, -45_n, +45_n, -45_n, +45_n]$  Composite plate subjected to impact loading. Geometry and mechanical properties

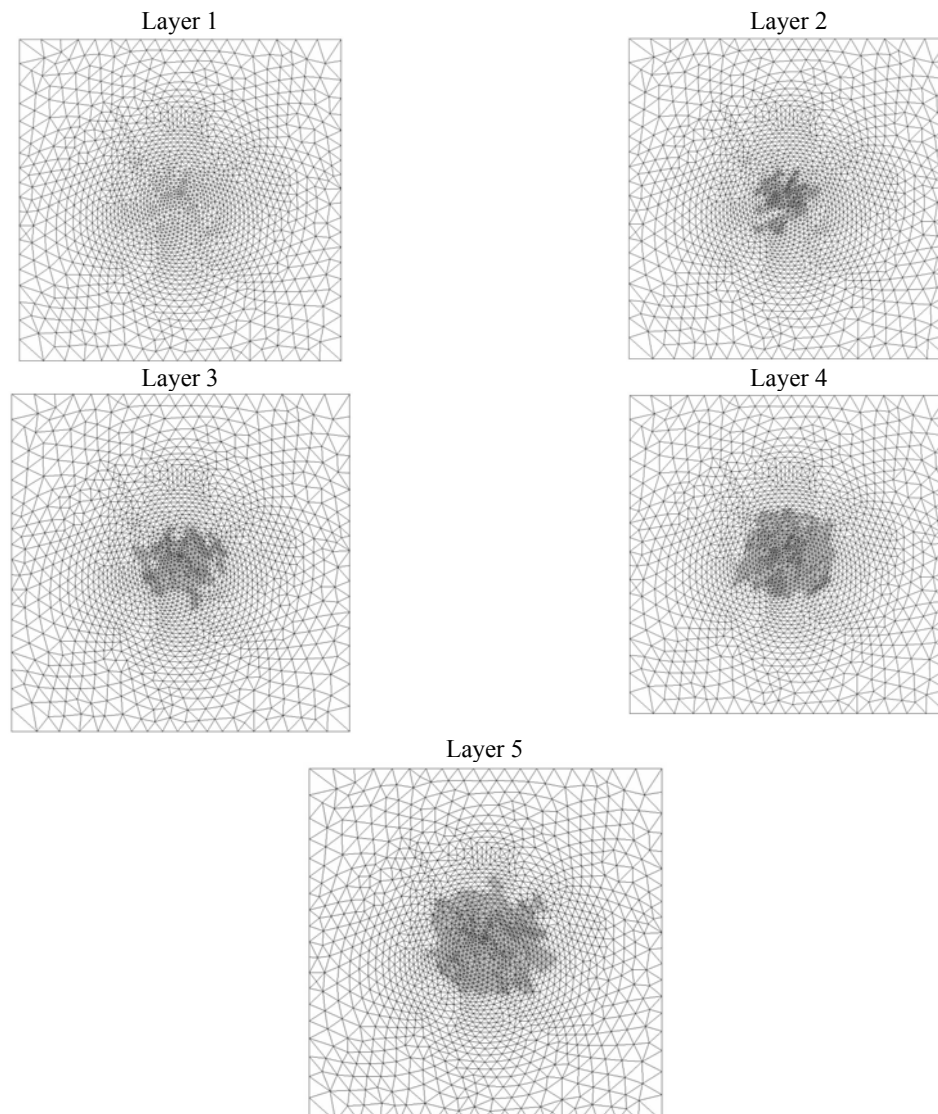


Fig. 14. Fracture patterns of different layers at  $t = 0.0136$  ms

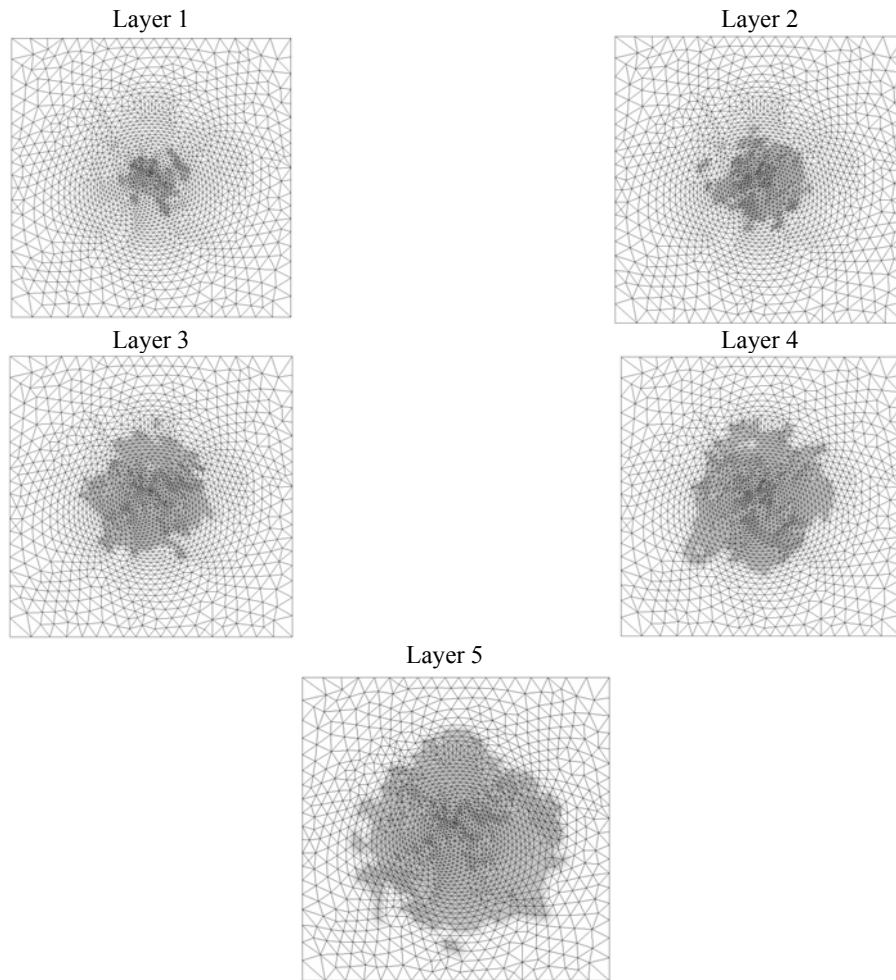


Fig. 15. Fracture patterns of different layers at  $t = 0.0362 \text{ ms}$

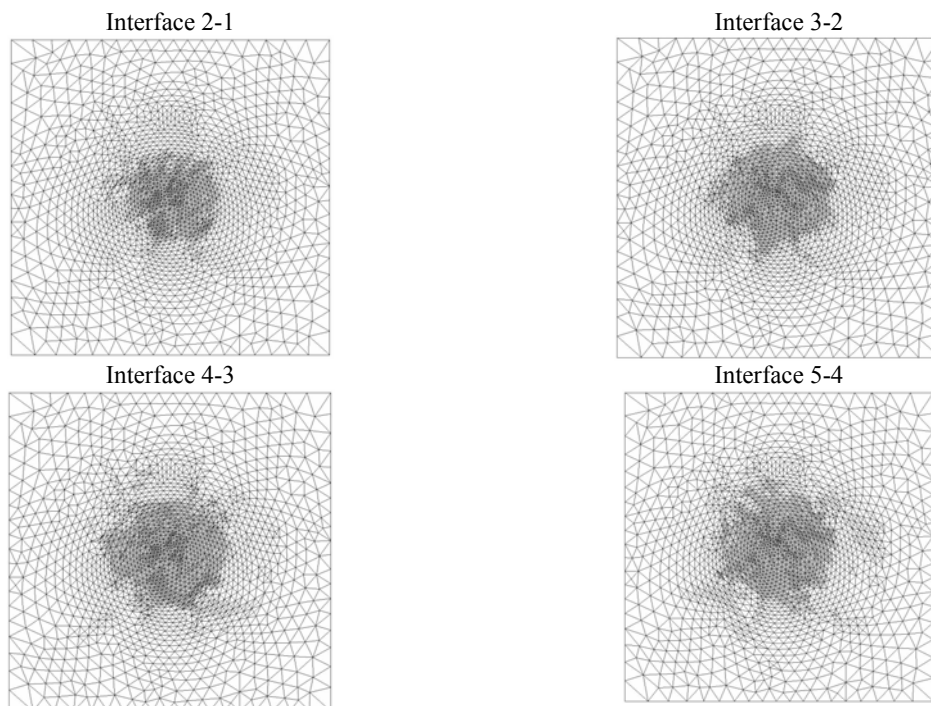


Fig. 16. Delamination patterns at different layer interfaces at  $t = 0.0362 \text{ ms}$

## REFERENCES

1. Belytschko, T. & Bindeman, L. P. (1991). Assumed strain stabilization of the 4-node quadrilateral with 1-point quadrature for nonlinear problems. *Computer Methods in Applied Mechanics and Engineering*, 88, 311-340.
2. Belytschko, T., Ong, J., Liu, W. K. & Kennedy, J. M. (1984a). Hourglass control in linear and nonlinear problems. *Computer Methods in Applied Mechanics and Engineering*, 43, 251-276.
3. Doherty, W. P., Wilson, E. L. & Taylor, R. L. (1969). *Stress analysis of axisymmetric solids utilizing higher order quadrilateral finite elements*. Tech. rept. Dept. of Civil Engineering, University of California, Berkeley. SESM Rept. No. 69-3.
4. Wilson, E. L., Taylor, R. L., Doherty, W. P. & Ghaboussi, J. (1973). Incompatible displacement models. *Pages 43-58 of: Fenves, S. J., Perrone, N., Robinson, A. R. & Schnobrich, W. C. (eds), Numerical and computer methods in structural mechanics*. Academic Press.
5. Taylor, R. L., Beresford, P. J. & Wilson, E. L. (1976). A non-conforming element for stress analysis. *International Journal for Numerical Methods in Engineering*, 10, 1211-1219.
6. Flanagan, D. P. & Belytschko, T. (1981). A uniform strain hexahedron and quadrilateral with orthogonal hourglass control. *International Journal for Numerical Methods in Engineering*, 17, 679-706.
7. Belytschko, T. & Tsay, C. S. (1983). A stabilization procedure for the quadrilateral plate element with one-point quadrature. *International Journal for Numerical Methods in Engineering*, 19, 405-419.
8. Belytschko, T. & Bachrach, W. E. (1986). Efficient implementation of quadrilaterals with high coarse-mesh accuracy. *Computer Methods in Applied Mechanics and Engineering*, 54, 279-301.
9. Stainier, L. & Ponthot, J. Ph. (1994). An improved one-point integration method for large strain elastoplastic analysis. *Computer Methods in Applied Mechanics and Engineering*, 118, 163-177.
10. Belytschko, T. & Leviathan, I. (1994). Physical stabilization of the 4-node shell element with one point quadrature. *Computer Methods in Applied Mechanics and Engineering*, 113, 321-350.
11. Belytschko, T. & Bindeman, L. P. (1993). Assumed strain stabilization of the eight node hexahedral element. *Computer Methods in Applied Mechanics and Engineering*, 105, 225-260.
12. Liu, W. K., Ong, J. S. J. & Uras, R. A. (1985a). Finite element stabilization matrices-a unification approach. *Computer Methods in Applied Mechanics and Engineering*, 53, 13-46.
13. Liu, W. K., Belytschko, T., Ong, J. S. J. & Law, S. E. (1985b). Use of stabilization matrices in nonlinear analysis. *Engineering Computations*, 2, 47-55.
14. Zhu, Y. Y. & Cescotto, S. (1996). Unified and mixed formulation of the 8-node hexahedral elements by assumed strain method. *Computer Methods in Applied Mechanics and Engineering*, 129, 177-209.
15. Koh, B. C. & Kikuchi, N. (1987). New improved hourglass control for bilinear and trilinear elements in anisotropic linear elasticity. *Computer Methods in Applied Mechanics and Engineering*, 65, 1-46.
16. Jetteur, Ph. & Cescotto, S. (1991). A mixed finite element for the analysis of large inelastic strains. *International Journal for Numerical Methods in Engineering*, 31, 229-239.
17. Liu, W. K., Chang, H., Chen, J. S. & Belytschko, T. (1988). Arbitrary Lagrangian-Eulerian Petrov-Galerkin finite elements for nonlinear continua. *Computer Methods in Applied Mechanics and Engineering*, 68, 259-310.
18. Simo, J. C. & Hughes, T. J. R. (1986). On the variational foundations of assumed strain methods. *Journal of Applied Mechanics*, 53, 51-54.
19. Li, K. P. & Cescotto, S. (1997). An 8-node brick element with mixed formulation for large deformation analyses. *Computer Methods in Applied Mechanics and Engineering*, 141, 157-204.
20. MacNeal, R. H. (1994). *Finite elements: Their design and performance*. Marcel Dekker Inc.
21. Mohammadi, S., Owen, D. R. J. & Peric, D. (1998). A combined finite/discrete element algorithm for delamination analysis of composites. *Finite Elements in Analysis and Design*, 28, 321-336.

22. Mohammadi, S., Foroozan-sepehr, S. & Asadollahi, A. (2002). Contact based delamination and fracture analysis of composites. *Thin Walled Structures*, 40, 595-609.
23. Owen, D. R. J. & Hinton, E. (1980). *Finite elements in plasticity: Theory and practice*. Pineridge Press.
24. Belytschko, T., Wong, B. L. & Chiang, H. Y. (1992). Advances in one-point quadrature shell elements. *Computer Methods in Applied Mechanics and Engineering*, 96, 93-107.
25. Balmer, H. A. & Witmer, E. A. (1964). *Theoretical-experimental correlation of large dynamic permanent deformation of impulsively loaded simple structures*. Tech. Rept. Air Force Flight Dynamics Laboratory. Report FDP-TDR-64-108.
26. Belytschko, T., Lin, J. T. & Tsay, C. S. (1984b). Explicit algorithms for the nonlinear dynamics of shells. *Computer Methods in Applied Mechanics and Engineering*, 42, 225-251.
27. Worswick, M. J., Strazincky, P. V. & Majeed, O. (1995). Dynamic fracture of fiber reinforced composite coupons. Pages 29-41 of: Sun, C.T., Sankar, B. V. & Rajapakse, Y.D.S. (eds), *Dynamic response and behaviour of composites*. ASME AD-46.